Deactivation of Ni spinel derived catalyst during the oxidative steam reforming of raw bio-oil

Aitor Arandia [a,b], Aingeru Remiro [a,*], Beatriz Valle [a], Javier Bilbao[a] and Ana G. Gayubo[a]

[a]*Department of Chemical Engineering, University of the Basque Country (UPV/EHU), P.O. Box 644-48080, Bilbao, Spain*

[b]*Department of Chemical and Metallurgical Engineering, School of Chemical Engineering, Aalto University, 02150, Espoo, Finland*

[*]*e-mail: aingeru.remiro@ehu.eus Phone: +34946015361. Fax:+34946013500*

Abstract

Deactivation of a bulk catalyst derived from $NiAl_2O_4$ spinel during the oxidative steam reforming (OSR) of raw bio-oil has been studied. The experiments were performed in a continuous system with two units in series: a thermal treatment unit at 500 ºC for the controlled deposition of pyrolytic lignin, and a fluidized bed reactor (700 ºC; S/C, 6; O/C, 0.34; space time, 0.15 $g_{catalyst}h \cdot g_{bio\text{-}oil}^{-1}$; time on stream, 1, 2, 4 and 6 h) for the OSR of the remaining oxygenates. The deactivation affects the reforming of bio-oil oxygenates according to their reactivity (from lower to higher), with the reforming of phenols being rapidly affected. The causes of deactivation are: i) coke deposition on the Ni^0 sites and on the Al_2O_3 support (6 wt % of each coke type after 6 h on stream), and; ii) sintering of Ni^0 crystals (with an increase in crystal size from 10.8 to 17.7 nm (measured by TEM)). The catalyst deactivation rate increases with time on stream, with the bio-oil oxygenates being the main coke precursors.

Keywords: bio-oil, hydrogen, oxidative steam reforming, Ni catalyst, deactivation, coke

1. Introduction

The large-scale use of H_2 as a primary energy carrier is a priority to meet the energy demand during the transition towards the development of innovative and sustainable energy systems based on renewable sources (solar, wind, hydro, etc.) [1,2]. In this scenario, the sustainable production of H_2 from lignocellulosic biomass, which minimizes net CO_2 emissions, is receiving a great deal of attention [3]. H_2 can be directly produced either by hydrolysis, gasification and pyrolysis of biomass or by reforming intermediate products, such as sugars, alcohols, and bio-oil [4]. Steam reforming (SR) of bio-oil (liquid product of biomass fast pyrolysis) is an attractive alternative for H_2 production which avoids the costly elimination of the high water content and enables the joint valorization of the complex mixture of oxygenated organic compounds contained in bio-oil [5-8]. High yield of bio-oil can be obtained by fast pyrolysis of biomass using widespread and well-developed technologies with low environmental impact [9,10].

The industrial implementation of bio-oil SR is curtailed by the high energy requirements due to its endothermic nature. The co-feeding of O_2 along with steam in an oxidative steam reforming process (OSR) would contribute to reduce these energy requirements [11,12]. Moreover, oxidation into CO_2 mitigates the production of CO, which is a desired quality for fuel-cell systems. The overall stoichiometry of bio-oil OSR reaction is given by Eq. (1):

$$C_nH_mO_k + pO_2 + (2n-k-2p)\ H_2O \rightarrow nCO_2 + (2n+m/2-k-2p)\ H_2 \quad (1)$$

One of the main challenges for the large-scale implementation of bio-oil OSR is to maintain the catalyst stability. This can be achieved by using stable and regenerable catalysts, as well as reaction equipment and operating conditions that minimize deactivation. Accordingly, advances in the SR of bio-oil [13], as well as in the steam or dry reforming of pure oxygenates and hydrocarbons are especially relevant.

Ni-based catalysts are the most used in the reforming processes due to their low cost and relative high stability in the presence of steam. These catalysts are mainly deactivated by blockage of the active sites (Ni^0 crystals) due to deposition of encapsulating coke [14], and by sintering of these metal sites [15-17].

The hydrothermal stability of Ni^0 sites is improved by doping these catalysts with alkaline and rare-earth metals, which attenuates coke deposition through the enhancement of water adsorption and gasification reactions [18-21].

Several authors have studied the effect of operating conditions (temperature and steam-to-carbon ratio) on deactivation of Ni supported catalysts in the steam reforming (SR) of bio-oil. Ochoa et al. [22] reported that formation of encapsulating coke is highly favored at 550 ºC, leading to a fast deactivation. Conversely, the coke deposited at 700 ºC is primarily composed of structured C deposited on the support, with a notably lower impact on deactivation. Other studies concluded that temperatures in the 650-700 ºC range are suitable for minimizing deactivation in the SR of raw bio-oil [23] or its bio-oil aqueous fraction [24]. The increase in steam-to carbon (S/C) ratio at moderate temperatures has a beneficial effect on catalyst deactivation, as it attenuates coke deposition due to promotion of coke gasification reactions [25]. Moreover, the effect of S/C ratio on catalyst deactivation is also associated with the agglomeration of metal particles when using high reforming temperatures. Thus, Sehested et al. [26,27] performed experimental analysis and simulations under typical SR conditions and concluded that the higher H_2O/H_2 ratio at 700 ºC, the higher sintering rate. In the same vein, Remiro et al. [24] reported almost negligible metal agglomeration at 600 ºC in the SR of bio-oil, whereas it is more significant at 700 ºC with high S/C ratios and substantial at 800 ºC even for low S/C.

The afore-mentioned works evidenced the role that deposition of pyrolytic lignin (PL) plays on the catalyst deactivation. This carbonaceous solid is formed by re-polymerization of phenolic oxygenates contained in bio-oil. The use of an original reaction system with two units in series, previously proposed by the authors, was proved to decrease the coke deposition on the catalyst, and therefore the deactivation rate [28]. This two-unit system consists of a thermal step for the controlled deposition of PL prior to the catalytic fluidized bed reactor, located in series for reforming the remaining oxygenates.

Although catalyst deactivation can be attenuated by using improved catalysts and suitable reaction conditions, it is an unavoidable effect. This fact involves that industrial implementation of raw bio-oil reforming would require suitable operating strategies, such as successive reaction-regeneration cycles

[17,29-31]. Consequently, establishing the reversible causes of deactivation is key to develop a suitable regeneration treatment, so that the catalyst would recover the activity of the fresh one. The bulk catalyst derived from $NiAl_2O_4$ spinel was proved to have a remarkable activity and selectivity for H_2 production in the OSR of bio-oil. In addition, it is fully regenerated by combustion of the coke in furnace at 850 °C, since the $NiAl_2O_4$ spinel structure of the fresh catalyst is completely recovered [32]. It should be pointed out that Ni supported catalysts undergo significant sintering of Ni^0 particles, which causes irreversible deactivation because the metallic dispersion is not recovered after coke combustion. This fact has been proven in the SR [33] and OSR of bio-oil [34].

The main objective of this paper is to gain knowledge on the deactivation mechanism of Ni spinel derived catalyst during the OSR of bio-oil, carried out at suitable reaction conditions (700 ºC, S/C = 6 and O/C = 0.34). For this purpose, the evolution with time on stream (TOS) of bio-oil conversion and product yields have been related to the deterioration of catalyst features, which have been thoroughly characterized by using several techniques. The porous structure has been determined by N_2 adsorption-desorption. The surface morphology and sintering of Niº metal species have been studied by X-ray diffraction (XRD) and Transmission Electron Microscopy (TEM). The amount and characteristics of the coke have been analyzed by Temperature Programmed Oxidation (TPO). The relationship between the evolution of kinetic results and the catalyst features enables to determine the significance and evolution of deactivation causes (coke deposition and sintering) with time on stream for this regenerable catalyst.

2. Material and methods

2.1. Catalyst and characterization techniques

The bulk $NiAl_2O_4$ spinel was synthesized by the co-precipitation method [35,36] using aqueous solutions of hexahydrated nickel nitrate ($Ni(NO_3)_2 \cdot 6H_2O$, Panreac, 99 %) and nona-hydrated alumina nitrate ($Al(NO_3)_3 \cdot 9H_2O$, Panreac, 98 %), and ammonium hydroxide as the precipitating agent (NH_4OH 0.6 M, Fluka, 5 M). After filtration, the precipitate was washed with distilled water to remove the

ammonium ions, then dried for 12 h, and calcined at 850 ºC for 4 h. The amount of Ni and Al nitrate salt precursors were those corresponding to 33 wt % of Ni (stoichiometric value for the $NiAl_2O_4$ spinel).

The physicochemical properties of fresh, reduced, and deactivated catalyst samples were characterized by several techniques. The specific surface area, average pore diameter and pore volume were determined by N_2 adsorption-desorption (*Autosorb iQ2* equipment from *Quantachrome)*. The X-ray diffraction (XRD) analyses were performed on a *Bruker D8 Advance* diffractometer with a CuKα1 radiation for studying the crystalline structure and determining the Ni average crystallite size by means of the Scherrer equation. The device is equipped with a Germanium primary monochromator, Bragg-Brentano geometry and with a CuKα1 wavelength of 1.5406 Å, corresponding to an X-ray tube with Cu anticathode. A Sol-X dispersive energy detector was employed, with a window optimized for CuKα1 for limiting the fluorescence radiation. Data collection was carried continuously, from 10º to 80° with step of 0.04° in 2θ and measurement time of 103 min.

The content, nature and location of the coke deposited on deactivated catalyst samples was analyzed by Temperature Programmed Oxidation (TPO) in a *Thermo Scientific TGA Q5000TA IR* thermobalance coupled in line with a mass spectrometer *Thermostar Balzers Instrument* for monitoring CO_2 signal. The TPO profile was quantified from the CO_2 signal, because oxidation of Ni during combustion might mask the thermogravimetric signal [32]. The procedure consisted on stabilization of the sample at 50 °C, followed by heating at 5 °C min^{-1} up to 800 °C under a stream of 50 cm^3 min^{-1} N_2 /O_2 (25 vol % of O_2).

The morphology of the coke was analyzed by transmission electronic microscopy (TEM) in a *Philips SuperTwin CM200* equipment. Likewise, the Ni particle size distribution (PSD) was determined by counting up to 300 individual metal particles in several TEM images for each catalyst sample.

2.2. Bio-oil composition

The raw bio-oil was supplied by *BTG Bioliquids BV* (Hengelo, The Netherlands). It was produced by flash pyrolysis of pine sawdust in a 5 ton-per-hour capacity plant provided with a conical rotary reactor. The density of raw bio-oil is 1.105 g ml^{-1} and its water content is 26 wt % (determined by Karl-Fischer

titration). Composition of oxygenates in the raw bio-oil and in the stream that enters the OSR reactor was analyzed by GC/MS (*Shimadzu QP2010S* device, provided with a *BPX-5* column of 50 m length, 0.22 mm diameter and 0.25 μm thick). The main compounds are acids, ketones, phenols, levoglucosan, esters, aldehydes, alcohols, and ethers (Table 1). Composition of the liquid produced at different TOS values was also analyzed with the aim of assessing whether the catalyst deactivation selectively affects the reforming of some oxygenated families in bio-oil.

2.3. Reaction equipment and operating conditions

The OSR experiments have been carried out in a continuous two-unit reaction equipment (*MicroActivity Reference* from *PID Eng&Tech*, described in detail elsewhere [28]) by feeding raw bio-oil. The first unit (thermal step) is a U-shaped steel tube (0.75 inch of ID), which is used for controlled vaporization of bio-oil and re-polymerization of oxygenates (mainly phenolic compounds derived from the pyrolysis of the biomass lignin). The temperature used in the thermal unit (500 ºC) was proven to be suitable for attaining a significant attenuation of catalyst deactivation, with a moderate decrease in the flow-rate of oxygenates that enters the catalytic reactor [37]. Thus, 16.5 wt % of the raw bio-oil oxygenates (on a water-free basis) are retained as pyrolytic lignin (PL). The second unit located in-line is the fluidized bed reforming reactor, where the catalyst is mixed with inert solid (SiC) (inert/catalyst mass ratio > 8/1) in order to ensure a suitable fluidization. Different particle size was used for the catalyst (between 150-250 μm) and the inert solid (< 40 μm) in order to facilitate their separation for the subsequent characterization of deactivated catalyst after each reaction.

An injection pump *(Harvard Apparatus 22)* was used for feeding the bio-oil (0.08 ml/min) and the additional water required to set the steam-to carbon (S/C) molar ratio was co-fed using a *307 Gilson pump*. Composition of the products stream was analyzed in-line using a *MicroGC 490 Agilent*, provided with 4 analytic channels: molecular sieve MS5 (for H_2, N_2, O_2, CH_4 and CO), Plot Q (for CO_2, H_2O and C_2-C_4 hydrocarbons), CPSIL (for C_5-C_{11} hydrocarbons, which were not detected in this work), and Stabilwax (for oxygenated compounds).

Prior to each OSR reaction, the catalyst was reduced in-situ under a H_2-N_2 stream (10 vol.% H_2) at 850 ºC for 4 h. These conditions assured complete reduction of $NiAl_2O_4$ spinel so that Ni^0 particles were well-dispersed on the Al_2O_3 support. The OSR reforming conditions were: atmospheric pressure; 700 ºC; space-time, 0.15 $g_{catalyst}h/g_{bio-oil}$; S/C ratio, 6; oxygen-to-carbon (O/C) molar ratio, 0.34. These values of temperature and S/C are suitable for maximizing the H_2 yield and catalyst stability. In previous works [22-25] it was stablished that sintering of Ni^0 crystals is noticeable above 700 ºC under OSR conditions. Moreover, a higher S/C ratio slightly improves H_2 yield but involves a significant increase in energy requirements for water vaporization. The increase in O/C ratio above 0.34 contributes to attenuate coke deposition, but reduces H_2 yield to unacceptable levels. It should be noted that a low space-time value was selected in order to have high catalyst deactivation conditions, so that meaningful results are rapidly obtained, which facilitates the comprehension of the deactivation mechanism in 6 h runs.

The OSR reactions have varying duration in order to analyze the evolution with TOS of products distribution and catalyst properties. After each experiment, the deactivated catalyst sample was characterized as described in Section 2.1. The liquid product collected at the end of each reaction (after draining the *Peltier* condenser) was analyzed by CG/MS. Thus, the composition of non-reacted oxygenates would provide information on their selective deactivation.

2.4. Reaction indices

The kinetic behavior of the catalyst was quantified by the following equations:

The conversion of bio-oil oxygenates (denoted as bio-oil conversion):

$$X_{bio\text{-}oil} = \frac{F_{in} - F_{out}}{F_{in}} \quad (2)$$

where F_{in} is the C molar flow-rate in bio-oil oxygenates at the reactor inlet (after subtracting the C retained with the pyrolytic lignin deposited in the thermal unit), F_{out} is the C molar flow-rate of bio-oil oxygenates at the reactor outlet (calculated from the molar fraction of oxygenates quantified by GC, and the total mole number quantified by C mass balance in the reforming reactor).

The yield of H_2 is referred to the stoichiometric maximum:

$$Y_{H_2} = \frac{F_{H_2}}{F^{o}_{H_2}} \quad (3)$$

where F_{H2} is the H_2 molar flow-rate in the product stream and F^{0}_{H2} is the stoichiometric flow-rate, which is 2.18 F_{in}. This value was calculated according to Eq. (1) and considering the average molecular formula of the bio-oil entering the reforming reactor ($C_{4.1}H_{6.9}O_{2.7}$, on a water-free basis). This formula was estimated by considering the elemental composition of the raw bio-oil ($C_{4.6}H_{6.2}O_{2.4}$) and the amount and elemental composition of the pyrolytic lignin ($C_{7.1}H_{2.8}O_{11.6}$) retained in the thermal step.

The yield of carbon-containing products (CO_2, CO, CH_4 and hydrocarbons) was quantified as:

$$Y_i = \frac{F_i}{F_{in}} \quad (4)$$

where the term F_i refers to the C molar flow-rate of each C-containing product, i.e., CO_2, CO, CH_4 and light hydrocarbons (mainly ethene and propene) (HCs). These latter result from the cracking/decomposition reactions of bio-oil.

3. Results

The cause-effect relationship of catalyst deactivation has been studied in order to gain knowledge on the deactivation mechanism of the bulk Ni spinel catalyst. The effect that deactivation has on bio-oil conversion and product yields, as well as on the reforming of each bio-oil oxygenated family is studied in Section 3.1 and 3.2, respectively. These results are explained by the evolution of the catalyst properties (as a result of the coke deposition and Ni sintering) in Section 3.3.

3.1. Evolution with TOS of conversion and product yields

Fig. 1 shows the evolution with TOS of bio-oil conversion and product yields until a high catalyst deactivation is attained. At zero TOS, bio-oil is fully converted obtaining high yields of H_2 (0.79) and CO_2 (0.9), along with low yield of CO (≈ 0.1) and negligible CH_4 and HCs amounts.

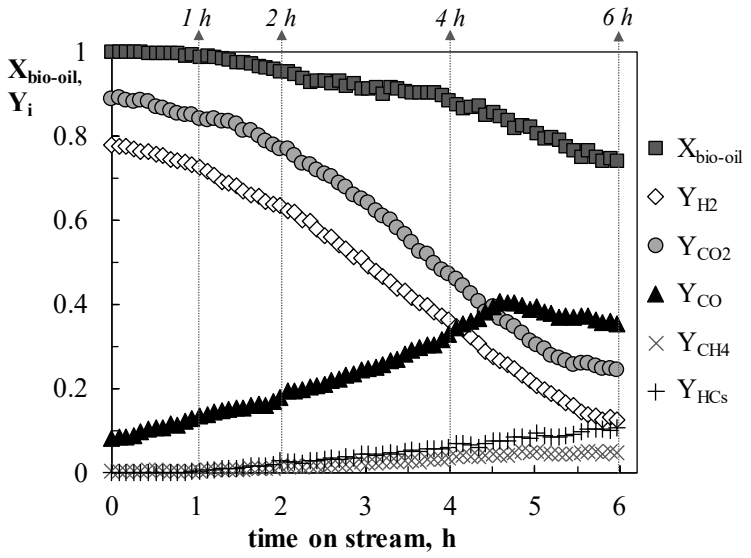

198

199 **Figure 1.** Evolution with TOS of bio-oil oxygenates conversion and products yields. Reaction
200 conditions: 700 ºC; S/C, 6; O/C, 0.34; space time, 0.15 $g_{catalyst}h \cdot g_{bio\text{-}oil}^{-1}$.

201 The yields of H_2 and CO_2 decrease with TOS, whereas CO yield increases up to 4.5 h TOS, which
202 evidences that WGS reaction (through which CO is converted into $CO_2 + H_2$) is rapidly affected by
203 deactivation, and to a greater extent than the reforming reaction of bio-oil oxygenates to form CO.
204 Nevertheless, as catalyst deactivation progresses the reaction rates of the reforming of bio-oil
205 oxygenates decrease and, consequently, the CO yield also decreases to the value corresponding to its
206 formation by thermal decomposition of the oxygenates. Meanwhile, bio-oil conversion and byproduct
207 yields (CH_4 and HCs) remain steady throughout 1 h, which suggests that reforming of oxygenates, CH_4
208 and hydrocarbons (formed by cracking) are less affected by deactivation. After 1h on stream, the latter
209 reaction indices evolve with TOS, following an almost linear trend after 2h on stream.

210 Based on these results, the duration of the different OSR reactions that were carried out to analyze the
211 coke deposition and characteristics of the deactivated catalyst were: 1 h, 2 h and 4 h (corresponding to
212 progressive deactivation states), and 6 h (deactivated catalyst, so that the reaction indices are similar to
213 those obtained in the reforming of bio-oil by thermal routes [38]).

214 ***3.2. Evolution with TOS of liquid product composition***

The catalyst deactivation selectively affects the reforming reactions of oxygenated compound families, according to their different reactivity and the catalyst capability for reforming them. As a result, composition of the liquid products (non-reacted oxygenates and water) varies with TOS. The composition of the liquid collected in this work at different TOS values (quantified by GC/MS as described in Section 2.2) is shown in Table 1.

Table 1. Yield and composition of oxygenates (on a water-free basis) in the raw bio-oil, in the stream that enters the OSR reactor**,** and in the liquid produced at different TOS values. Reaction conditions: 700 ºC; S/C, 6; O/C, 0.34; space time, 0.15 $g_{catalyst}h \cdot g_{bio\text{-}oil}^{-1}$.

Compounds	**raw bio-oil**	**Reactor inlet**	**1 h**	**2 h**	**4 h**	**6 h**
Yield of oxygenates	-	-	0.1	5	11	26
Ketones	15.55	37.32	35.63	15.14	17.32	12.58
acetone	*1.8*	*10.05*	*35.63*	*9.97*	*10.93*	*6.12*
1-hydroxy-2-propanone	*7.44*	*20.38*	-	*4.77*	*5.86*	*5.26*
Acids	35.32	45.96	20.27	45.89	43.69	49.44
acetic acid	*17.07*	*35.53*	*20.27*	*45.89*	*43.69*	*47.49*
Esters	9.41	2.13	-	1.52	1.52	2.15
Aldehydes	6.24	3.08	-	0.46	0.51	1.52
Phenols	15.36	6.51	44.1	33.4	32.71	29.86
phenol	*0.31*	*1.77*	*23.59*	*18.16*	*18.56*	*13.59*
2-methylphenol	*0.73*	*1.86*	*15.51*	*10.75*	*9.84*	*9.35*
Ethers	0.48	0.72	-	0.91	1.38	0.91
Alcohols	2.55	-	-	-	-	-
Levoglucosan	10.9	2.82	-	-	-	-
Others	4.19	1.46	-	-	-	-
Not identified	-	-	-	2.69	2.87	3.54

After 1 h TOS the liquid is composed of acetone, acetic acid, and alkyl-phenols, with the concentration of the most reactive oxygenated compounds being negligible (Table 1). The presence of non-converted oxygenates in the product stream at 1 h TOS is consistent with the results of Fig. 1, which shows that the catalyst is slowly deactivated in this period. The great amount of acetone (highly reactive for reforming reactions) can be explained by ketonization of acetic acid (majority compound in the bio-oil) and to a lesser extent, of aldehydes, alcohols and esters [39]. The high concentration of alkyl-phenols (phenol and 2-methylphenol) can be attributed to cracking/decomposition reactions of guaiacols and catechols. These demethoxylation (DMO) and demethylation (DME/dehydration) reactions have been

explained in detail by Valle et al. [40]. Thermal reaction pathways (which do not require any catalyst to evolve) are expected to contribute to the products distribution at 700 ºC. This contribution is expected to be greater as the catalyst deactivates for reforming reactions, since the concentration of oxygenates in the reaction medium is higher.

Interestingly, the concentration of acetic acid increases notably between 1 and 2 h TOS (Table 1), whereas that of ketones and phenols decrease. The result is explained by the decrease in the reforming rate of acetic acid as a consequence of catalyst deactivation. The decrease in the reaction rate of acetic acid ketonization will also contribute to this result. Consequently, the concentration of ketones decreases between 1 and 2 h TOS, and that of acetic increases. This trend is attenuated between 2 and 6 h TOS, with the liquid fraction being mainly composed by acetic acid and phenols, because the effect of deactivation attenuates progressively.

3.3. Characterization of deactivated catalyst samples

3.3.1. Coke deposition

The TPO results of the coke deposited on the catalyst deactivated during reactions of different TOS are shown in Fig. 2a. Two different combustion domains are discerned in the TPO profiles, corresponding to a coke burning at low temperature (below 500 ºC, denoted Coke I), and to a coke burning at high temperature (above 500 ºC, denoted Coke II). Based on the literature that tackles the analysis of the coke deposited on supported metal catalysts by TPO [22,41-43], the Coke I is associated to a coke fraction deposited on the metal sites, which activate its combustion. The contribution of this type of coke to deactivation of the catalyst is well-known in the steam reforming of bio-oil, in which a small amount of coke encapsulates the metal sites, thus hindering the adsorption of reactants [22,41]. The Coke II is associated to a coke deposited on the support (in this case, the Al_2O_3 formed after reduction of the bulk spinel $NiAl_2O_4$). Combustion of this coke fraction is not catalyzed by metal sites. The temperature corresponding to the maximum of these peaks in the TPO profiles is also dependent on the degree of condensation (C/H ratio) and pore blockage, which are factors that hinder the combustion of the coke and increase the required temperature [22,44].

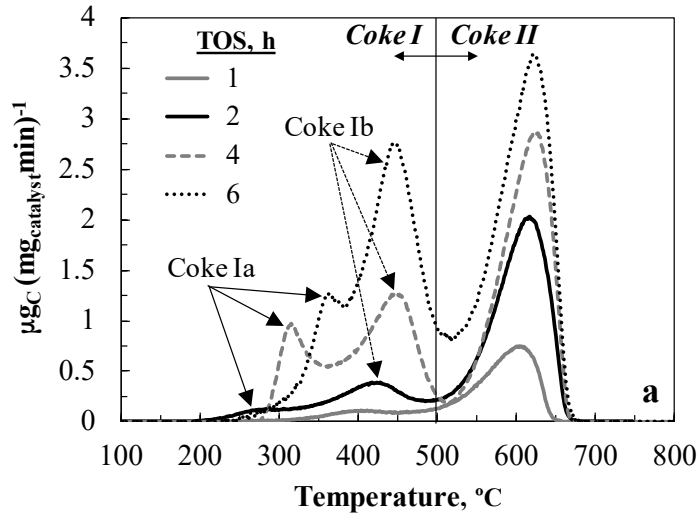

258

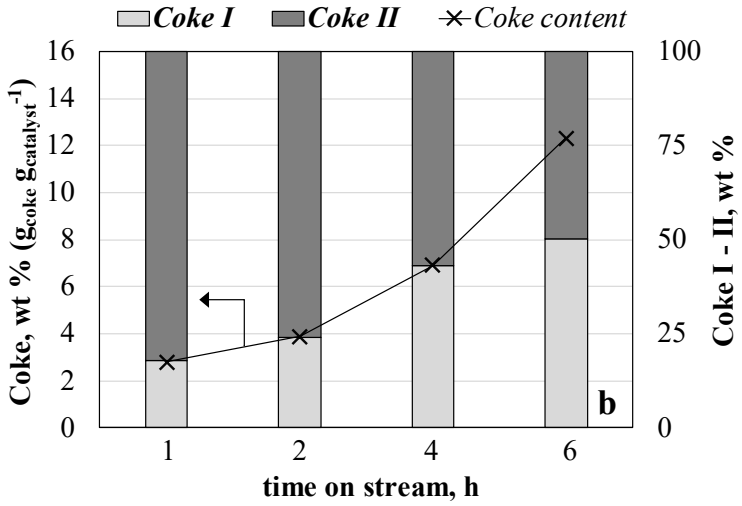

259

260 **Figure 2.** TPO profiles (a), total coke content and cokes I-II fractions (b) for the catalyst used at
261 different TOS. Reaction conditions: 700 ºC; S/C, 6; O/C, 0.34; space time, 0.15 $g_{catalyst}h \cdot g_{bio\text{-}oil}^{-1}$.

263 Interestingly, two different combustion peaks are discerned within Coke I in the TPO results
264 corresponding to the catalyst deactivated above 2 h TOS (Fig. 2a). These have been denoted as Coke Ia
265 and Coke Ib, according to their combustion temperature. This result can be explained by the particular
266 morphology of the bulk catalyst derived from Ni spinel. After the spinel reduction, the Ni^0 particles are
267 uniformly distributed over the catalyst particle (both inside the porous structure and in the surface).
268 Conversely, the synthesis methods of supported Ni catalysts usually originate Ni^0 particles preferably
269 located on the catalyst surface [32].

While there is no precedent in literature on different coke fractions in Ni spinel catalysts used in oxygenates reforming, it can presumably be considered that the coke deposited on the Ni sites located outside the catalyst particles (Coke Ia) can be discerned from the coke deposited on the Ni sites inside the particle (coke Ib), whose combustion kinetics would be limited by diffusion within the porous structure. The presence of two different combustion peaks within the combustion domain at low temperature (corresponding to encapsulating coke) has been also observed in the steam reforming of bio-oil over supported Ni catalysts [22,28,42,44,45]. According to Ochoa et al. [42], the presence of two combustion peaks in the Ni/La_2O_3-αAl_2O_3 catalysts is also explained by the different location and nature of the two coke fractions deposited on the Ni^0 crystals. Thus, the peak at lower combustion temperature (in the 340-370 ºC range, depending on the reaction conditions) corresponds to a surface layer of encapsulating coke with less condensed carbonaceous structure, higher oxygen content and lower activation energy. The peak burning at higher temperature (in the 400-430 ºC range) corresponds to inner layers of encapsulating coke, whose combustion needs higher temperature and activation energy.

The three combustion peaks increase as the coke deposition evolves (Fig. 2a). For the sake of clarity, the evolution with TOS of total coke content and the relative content of Coke I and Coke II are shown in Fig. 2b. Although the Coke II is predominant for short reaction times, deposition of coke on the Ni sites (Coke I) becomes increasingly important as the TOS increases, so that the content of both coke fractions is the same at the end of reaction. Besides, a slight increase in combustion temperatures is also observed in Fig. 2a as the TOS is raised, suggesting a higher condensation degree of carbon structures [42]. This increase is less noticeable for Coke II (which shifts from 605 °C to 630 °C), is more significant for Coke Ib (between 400 ºC and 450 °C) and is remarkable for Coke Ia (which shifts from 260 °C at 2 h TOS to 360 °C at 6 h). This result reveals that Coke Ia fraction (deposited on the Ni^0 crystals) gains a higher degree of condensation with TOS. Consequently, the peaks corresponding to Coke Ia and Coke Ib tend to meet at a single peak for high values of TOS and coke content.

The comparison of results in Fig. 1 and Table 1 with those reported in Fig. 2 allows establishing a relationship between the evolution of compounds in the reaction medium and the formation of each type of coke, and thereby identifying their possible precursors. Thus, the prevailing coke fraction at 1 h TOS

297 is Coke II, whose formation can be attributed to the degradation of bio-oil oxygenates adsorbed on the
298 Al_2O_3 support towards more condensed carbonaceous structures, while the Coke I would be formed
299 from the oxygenates adsorbed on the Ni^0 crystals. The increasing deposition of Coke I (deposited on the
300 Ni sites) above 2h TOS (Fig. 2) may be related to the remarkable increase of non-converted oxygenates
301 in the reaction medium (the oxygenates conversion decreases from 96 % at 2 h to 70 % at 6 h TOS).
302 This coke encapsulates the Ni sites and contributes to the complete deactivation of the catalyst for the
303 reforming reactions after 6 h TOS. Similarly, the increasing amount of non-converted oxygenates in the
304 reaction medium contributes to the progressive increase in Coke II (on the Al_2O_3 support) with TOS.

305 Furthermore, decomposition reactions of CH_4 and HCs could also contribute to coke formation above 2
306 h TOS, since their presence in the reaction medium begins to be appreciable. These compounds have
307 been reported as precursors of a filamentous coke in the literature concerning the reforming of methane,
308 pure oxygenates, and hydrocarbons. This type of coke is deposited on supported Ni catalysts preferably
309 at temperatures between 500-650 °C [46-51]. Nevertheless, the formation of filamentous coke on the Ni
310 spinel catalyst is not favored under the conditions used in this work for the OSR of bio-oil, at high
311 temperature (700 ºC). Thus, no carbon filament is identified in the TEM images of the catalyst
312 deactivated after different reaction times (Fig. 3), neither in the most deactivated catalyst (Fig. 3j) for
313 which the coke seems to be completely amorphous. Consequently, there is no evidence of the
314 mechanism of filamentous coke formation from these compounds in the SR of bio-oil at 700 ºC over
315 the Ni spinel derived catalyst. Moreover, despite the increasing concentration of CO above 2 h TOS, the
316 Boudouard reaction is not expected to contribute to coke deposition under the conditions of this work
317 (700 ºC) due to its exothermic nature [46].

318

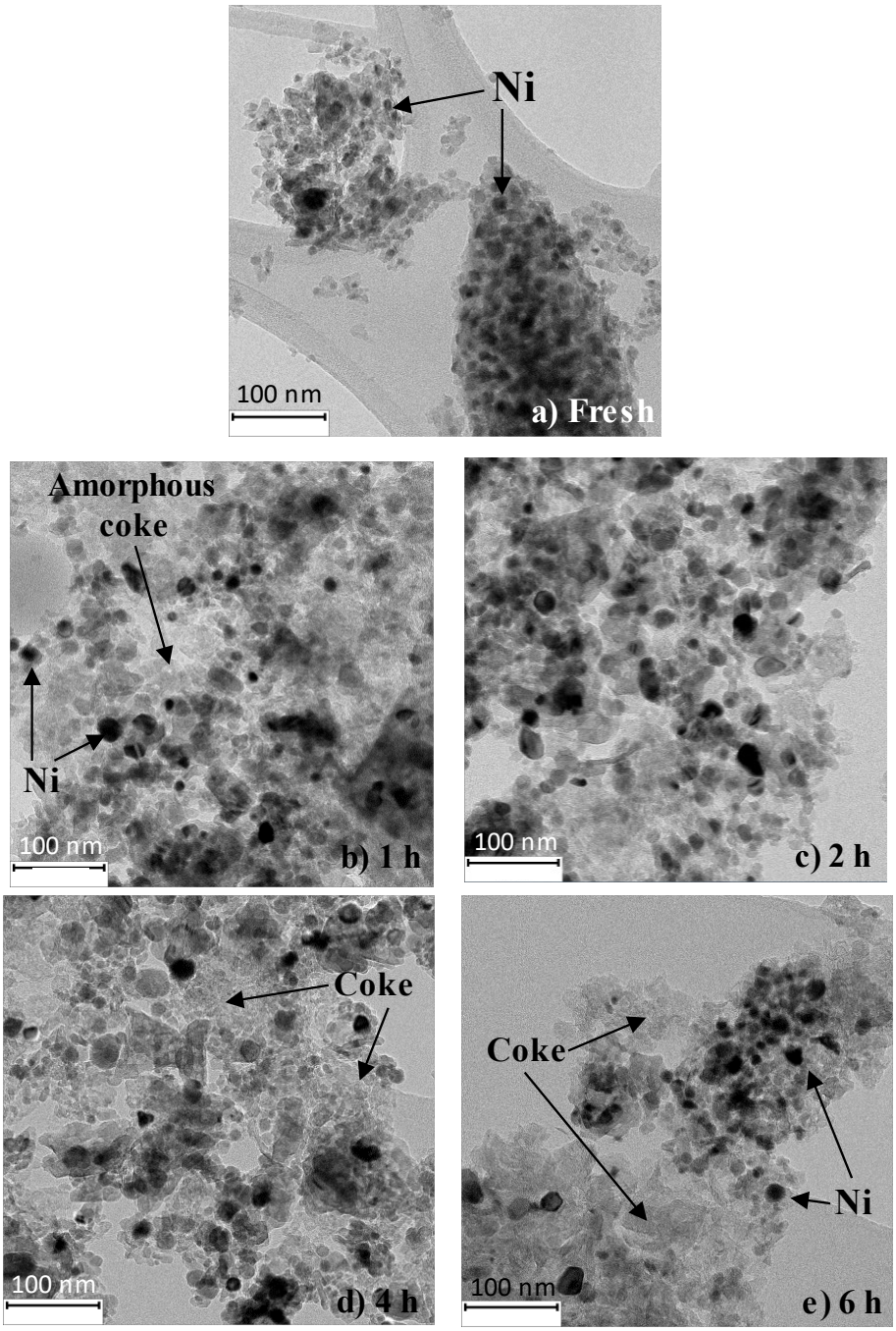

Figure 3. TEM images of fresh-reduced and samples of catalyst used at different TOS. Reaction conditions: 700 ºC; S/C, 6; O/C, 0.34; space time, 0.15 $g_{catalyst}h \cdot g_{bio\text{-}oil}^{-1}$.

3.3.2. Evolution of physical and metallic properties of the catalyst

The BET surface area, pore volume and average pore diameter corresponding to the fresh-reduced catalyst and the catalyst samples with different deactivation degree are shown in Table 2. Both the BET surface area and the pore volume decrease with TOS, thus revealing partial blockage of the Al_2O_3

mesoporous structure due to the deposition of a low-porous coke [52,53]. The slight increase in the average pore size as the coke deposition evolves suggests a certain preference for deposition on smaller mesopores. The deterioration of the physical properties in Table 2 is consistent with the evolution of coke deposition and its effect on catalyst deactivation (Fig. 1).

Table 2. Physical properties of fresh-reduced and samples of catalyst used at different TOS. Reaction conditions: 700 ºC; S/C, 6; O/C, 0.34; space time, 0.15 $g_{catalyst}h \cdot g_{bio\text{-}oil}^{-1}$.

TOS, h	S_{BET}, m^2g^{-1}	V_{pore}, cm^3g^{-1}	d_{pore}, nm
(Fresh-reduced)	80.2	0.316	14.3
1	70.9	0.293	15.1
2	69.4	0.275	16.5
4	67.6	0.256	16.8
6	59.6	0.252	16.9

The results of Ni^0 particle size distribution (PSD) calculated from the TEM images (Fig. 3) are shown in Fig. 4. These results reveal small, well-defined and homogeneously dispersed Ni particles on the fresh-reduced catalyst, whereas the Ni particles are bigger and more heterogeneously distributed as the TOS is increased. Accordingly, the Ni particle size after 6 h TOS is in the 10-30 nm range, and particles above 30 nm are not detected. It should be also noted that agglomeration of particles occurs predominantly at the beginning of reaction, with an increase in the average particle size from 10.8 nm to 14.5 nm after 1 h TOS. Then, the sintering rate is lower and the PSD tends towards steady values.

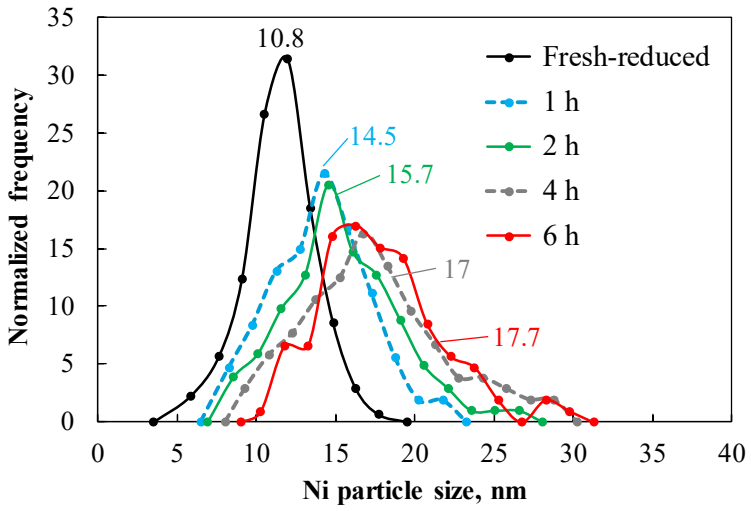

342 **Figure 4.** Particle size distribution (PSD) of Ni^0 crystals and average particle size obtained from TEM
343 images of fresh-reduced and samples of catalyst used at different TOS Reaction conditions:
344 700 ºC; S/C, 6; O/C, 0.34; space time, 0.15 $g_{catalyst}h \cdot g_{bio\text{-}oil}^{-1}$.

345 Table 3 shows the evolution with TOS of the average Ni^0 particle size, determined by means of Debye-
346 Scherrer equation at $2\theta = 51.8$ º from the corresponding X-ray diffractograms (not shown). It should be
347 pointed out that NiO phase was not detected in XRD diffractograms, which evidences two facts: i)
348 despite the oxidizing effect of O_2, there is a highly reductive atmosphere in the reaction medium (with
349 high concentration of H_2, especially at the beginning of reaction) that maintains the Ni metal in its active
350 reduced state; ii) the encapsulating coke capability of preserving the Ni^0 state when the catalyst is
351 exposed to the atmosphere (i.e., when removed from the reactor to carry out the XRD analysis) [54].
352 The results shown in Table 3 are consistent with those in Fig. 3 and Fig. 4. According to the values in
353 Table 3, the Ni average particle size in the catalyst deactivated after 6 h TOS is about 37 % greater than
354 in the fresh-reduced sample (from 11.7 nm up to 16 nm). Based on the size distribution determined from
355 TEM results (Fig. 4), which is a more accurate measurement of the average particle size, the Ni^0 particle
356 size in the catalyst at 6 h TOS is about 63 % greater (from 10.8 to 17.7 nm).

357 **Table 3.** Evolution with TOS of the average Ni particle size, estimated by XRD diffractograms in the
358 diffraction angle 51.8 º (plane 2 0 0). Reaction conditions: 700 ºC; S/C, 6; O/C, 0.34; space
359 time, 0.15 $g_{catalyst}h \cdot g_{bio\text{-}oil}^{-1}$.

360

TOS, h	**dNi^0, nm** 51.8 º, *plane (2 0 0)*
(Fresh-reduced)	11.7
1	13.8
2	14.5
4	15.1
6	16.0

361

362

363

364 The Ni sintering observed in the afore mentioned results can be attributed to the high reaction
365 temperature (700 ºC) and the high water content in the reaction medium. Thus, Ni atoms show signs of

mobility above 590 ºC (Ni Tamman temperature, half of the melting point temperature), which leads to agglomeration of metal particles [7]. In addition, the high content of steam in the reaction medium promotes the evolution of sintering mechanisms of metal and support [27,55].

4. Discussion

Characterization by TPO, XRD and TEM of the catalyst deactivated for different values of TOS evidences changes in the physicochemical and morphological properties during the OSR reaction of bio-oil. These changes are a consequence of the evolution of both causes of deactivation, i.e., coke deposition and Ni sintering, schematically outlined in Fig. 5. Each deactivation cause evolves at a different rate and has a different impact on the catalyst deactivation. Thus, coke is deposited both on the Ni^0 crystals located in the surface of the Al_2O_3 support (formed after reduction of the Ni-Al spinel catalyst) (Coke Ia) and on those located inside the Al_2O_3 (Coke Ib), encapsulating the Ni sites and leading to catalyst deactivation. Likewise, coke is also deposited on the Al_2O_3 support (Coke II) leading to a partial pore blockage, which also contributes to the catalyst deactivation because it hinders the access of the reactants to the Ni^0 sites located inside the porous structure of the Al_2O_3 support.

The initial coke deposition, which occurs preferably far from the Ni sites (Coke II), can be attributed to the presence of bio-oil oxygenates in the reaction medium. However, as the concentration of these oxygenates increases in the reaction medium, there is a faster coke formation on the Ni^0 sites (Coke Ia and Coke Ib), with the consequent increase in the deactivation rate. The relationship between the oxygenates concentration and the formation of both types of Coke I is difficult to explain because the increasing concentration of each type of oxygenate throughout reaction depends on its reactivity and also on secondary reactions (thermal and dehydroxygenation).

Furthermore, although coke formation by decomposition of CH_4 and HCs could be considered when the concentration these compounds is significant (due to the catalyst deactivation for their reforming reactions), this is not likely to occur since these reactions are not favored under the conditions used in this work. In addition, the formation of the characteristic carbon filaments is not observed. Anyway,

coke formation through these reactions would not have an important relevance since it would occur when the catalyst is highly deactivated.

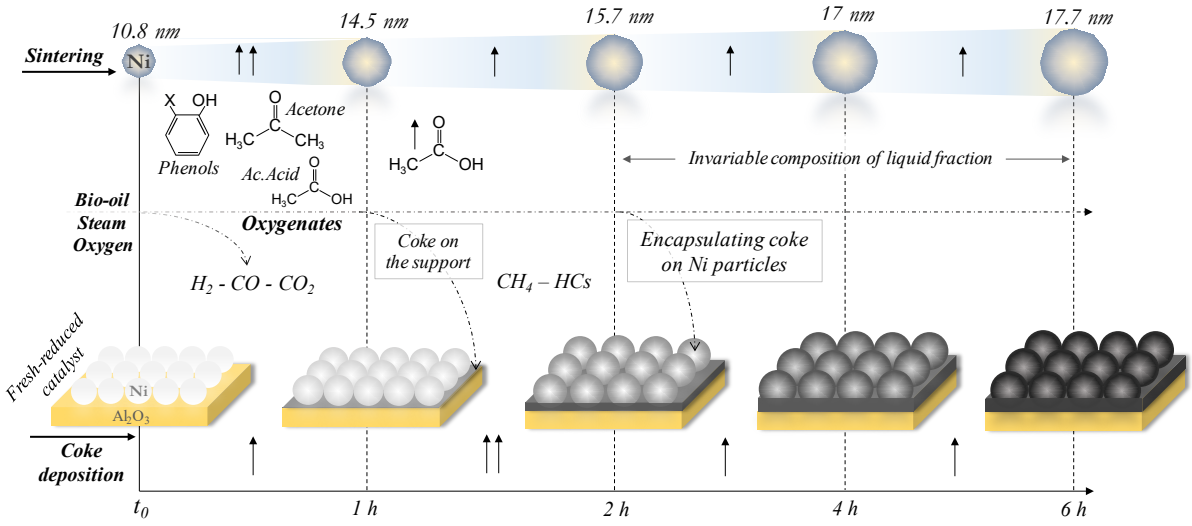

Figure 5. Deactivation scheme of catalyst based on Ni morphological changes and coke evolution with TOS. Reaction conditions: 700 ºC; S/C, 6; O/C, 0.34; space time, 0.15 $g_{catalyst}h \cdot g_{bio\text{-}oil}^{-1}$.

Similarly, the increase in Ni^0 particle size evidences a significant sintering. It is a well-known fact that the activity of Ni based catalysts in the reforming reactions is strongly dependent on the metal dispersion and size of the crystals [56]. Besides, there is a synergy between mechanisms of Ni sintering and coke formation, as this latter is accelerated by increasing the crystal size [57,58]. It should be noted that the sintering degree observed in this work for the catalyst derived from bulk $NiAl_2O_4$ spinel (with Ni^0 size increasing from 10.8 nm to 17.7 nm in 6 h on stream) is similar to that previously reported by Remiro et al. [33] in the OSR of bio-oil with supported Ni/La_2O_3-αAl_2O_3 catalyst (calcined at 550 ºC). The Ni^0 size in this supported catalyst increased from 7.0 nm to 12.6 nm in 4 h on stream for the same temperature used in this work (700 °C). Although for both catalysts the degree of Ni sintering is similar, the contribution of this sintering to catalyst deactivation is different. For the supported Ni/La_2O_3-αAl_2O_3 catalyst, there is insignificant coke deposition under conditions of high O/C ratio (0.67), with the Ni sintering being the main deactivation cause. Moreover, this deactivation is irreversible, because the catalyst does not recover the Ni dispersion after combustion of the coke, and therefore it does not recover the initial activity [34]. Conversely, the results of this work reveal that although Ni sintering contributes

410 to the deactivation of the bulk catalyst derived from $NiAl_2O_4$ spinel, coke deposition is the main
411 deactivation cause. In spite of the rapid deactivation, this is a more interesting catalyst for use in the
412 large-scale bio-oil OSR with strategies involving catalyst regeneration, because its deactivation is
413 reversible as has been previously reported [32]. This catalyst can be completely regenerated by coke
414 combustion with air at 850 ºC, since this high temperature enables a full recovery of the initial $NiAl_2O_4$
415 spinel structure. The subsequent reduction of the recovered spinel leads to highly dispersed and
416 homogeneously distributed Ni^0 particles in the bulk catalyst, so that it recovers the activity
417 corresponding to the fresh catalyst [32].

418 It should be noted that coke deposition results reported in this work correspond to reactions performed
419 with low value of space-time, since it was intended to promote coke formation in order to study the
420 rapid deactivation (within few hours of TOS). These results highlight the relevance of the concentration
421 of oxygenates in bio-oil on coke deposition rate. Based on this mechanism, conditions of full bio-oil
422 conversion (e.g., high space-time of catalyst) are advisable to avoid the presence of significant amount
423 of oxygenates (coke precursors) in the reaction medium. Thus, the catalyst deactivation is attenuated,
424 which is necessary for the operation to a higher scale.

425 **5. Conclusions**

426 Deactivation of a bulk catalyst derived from $NiAl_2O_4$ spinel during the oxidative steam reforming (OSR)
427 of bio-oil at 700 ºC differs from that reported for supported Ni catalysts. The Ni spinel catalyst is mainly
428 deactivated by coke deposition on the Ni^0 particles which progressively blocks these active sites. This
429 coke is composed of two fractions; one that is deposited on the Ni^0 sites located in the surface of the
430 Al_2O_3 support (formed from $NiAl_2O_4$ spinel reduction), and other deposited on the Ni^0 sites located
431 inside the porous structure of Al_2O_3. The deposition of other type of coke on the Al_2O_3 support that
432 causes partial blockage of the porous structure, also contribute to the catalyst deactivation. The catalyst
433 is completely deactivated with a content of 6 wt% of each type of coke (deposited in 6 h on stream under
434 the studied conditions). The relationship between the evolution of compounds concentration in the
435 reaction medium with the evolution of each coke fraction reveals that the bio-oil oxygenates are the
436 coke precursors. Moreover, the evolution of non-reformed oxygenates with time on stream shows that

437 the catalyst deactivation selectively affects the reforming of bio-oil oxygenates according to their
438 reactivity. Consequently, the reforming of phenolic compounds, acetic acid and acetone is rapidly
439 affected by deactivation. The sintering of Ni^0 sites also contributes to the deactivation, with an increase
440 in Ni^0 crystal size from 10.8 to 17.7 nm (measured by TEM).

441 Based on these results, although the accelerated deactivation conditions used in this work have been
442 adequate to facilitate understanding of the deactivation mechanism, on an industrial scale conditions of
443 full bio-oil conversion (with high space-time) are advisable to avoid the presence of significant amount
444 of oxygenates in the reaction medium. Therefore, the catalyst deactivation is attenuated and its useful
445 lifespan before replacement and subsequent regeneration is prolonged.

446

Acknowledgements

This work was carried out with the financial support of the Department of Education Universities and Investigation of the Basque Government (IT1218-19), the European Commission (HORIZON H2020-MSCA RISE 2018. Contract No. 823745) and the Ministry of Economy and Competitiveness of the Spanish Government jointly with the European Regional Development Funds (AEI/FEDER, UE) (Projects CTQ2015-68883-R and RTI2018-100771-B-I00) and Ph.D. grant BES-2013-063639 for A. Arandia).

References

[1] A. Ahmed, A.Q. Al-Amin, A.F. Ambrose, R. Saidur, Hydrogen fuel and transport system: A sustainable and environmental future, Int. J. Hydrogen Energy 40 (2016) 1369–1380. https://doi.org/10.1016/j.ijhydene.2015.11.084

[2] C. Acar, I. Dincer, Review and evaluation of hydrogen production options for better environment, J. Clean. Prod. 2018 (2019) 835–849. https://doi.org/10.1016/j.jclepro.2019.02.046

[3] E.S. Hanley, J-P. Deane, B.P. Ó Gallachóir, The role of hydrogen in low carbon energy futures–A review of existing perspectives, Renew. Sust. Energ. Rev. 82 (2018) 3027–3045. https://doi.org/10.1016/j.rser.2017.10.034

[4] A. Arregi, M. Amutio, G. Lopez, J. Bilbao, M. Olazar, Evaluation of thermochemical routes for hydrogen production from biomass: A review, Energy Convers. Manage. 165 (2018) 696–719. https://doi.org/10.1016/j.enconman.2018.03.089

[5] F. Seyedeyn-Azad, E. Salehi, J. Abedi, T. Harding, Biomass to hydrogen via catalytic steam reforming of bio-oil over Ni-supported alumina catalysts, Fuel Process. Technol. 92 (2011) 563–569. https://doi.org/10.1016/j.fuproc.2010.11.012

[6] S.A. Chattanathan, S. Adhikari, N. Abdoulmoumine, A review on current status of hydrogen production from bio-oil, Renew. Sust. Energ. Rev. 16 (2012) 2366–2372. https://doi.org/10.1016/j.rser.2012.01.051

[7] R. Trane, S. Dahl, M.S. Skjoth-Rasmussen, A.D. Jensen, Catalytic steam reforming of bio-oil. Int. J. Hydrogen Energy 37 (2012) 6447–6472. https://doi.org/10.1016/j.ijhydene.2012.01.023

[8] A.G. Adeniyi, K.S. Otoikhian, J.O. Ighalo, Steam reforming of biomass pyrolysis oil: A review, Int. J. Chem. React. Eng. 17 (2019) nº 20180328. https://doi.org/10.1515/ijcre-2018-0328

[9] R.E. Guedes, A.S. Luna, A.R. Torres, Operating parameters for bio-oil production in biomass pyrolysis: A review, J. Anal. Appl. Pyrolysis 129 (2018) 134–49. https://doi.org/10.1016/j.jaap.2017.11.019

[10] G. Perkins, T. Bhaskar, M. Konarova, Process development status of fast pyrolysis technologies for the manufacture of renewable transport fuels from biomass, Renew. Sust. Energy Rev. 90 (2018) 292–315. https://doi.org/10.1016/j.rser.2018.03.048

[11] S. Czernik, R. French, Distributed production of hydrogen by auto-thermal reforming of fast pyrolysis bio-oil, Int. J. Hydrogen Energy 39 (2014) 744–750. https://doi.org/10.1016/j.ijhydene.2013.10.134

[12] V. Paasikallio, A. Azhari, J. Kihlman, P. Simell, J. Lehtonen, Oxidative steam reforming of pyrolysis oil aqueous fraction with zirconia pre-conversion catalyst, Int. J. Hydrogen Energy 40 (2015) 12088–12096. https://doi.org/10.1016/j.ijhydene.2015.07.017

[13] J. Chen, J. Sun, Y. Wang, Catalysts for steam reforming of bio-oil: A review, Ind. Eng. Chem. Res. 56 (2017) 4627–4637. https://doi.org/10.1021/acs.iecr.7b00600

[14] L. Santamaria, A. Arregi, G. Lopez, M. Artetxe, M. Amutio, J. Bilbao, M. Olazar, Effect of La_2O_3 promotion on a Ni/Al_2O_3 catalyst for H_2 production in the in-line biomass pyrolysis-reforming, Fuel, in press. https://doi.org/10.1016/j.fuel.2019.116593

[15] J.J. Spivey, Deactivation of reforming catalysts, in: D. Shekhawat, J.J. Spivey, D.A. Berry (Eds.) Fuel cells: Technologies for Fuel Processing, Elsevier, 2011, pp. 285–315. https://doi.org/10.1016/B978-0-444-53563-4.10010-0

[16] J. Pasel, S. Wohlrab, S. Kreft, M. Rotov, K. Löhken, R. Peters, D. Stolten, Routes for deactivation of different autothermal reforming catalysts, J. Power Sources 325 (2016) 51–63. https://doi.org/10.1016/j.jpowsour.2016.06.005

[17] C.V. Satyanarayana, D. Srikant, H.R. Gurav, Chapter 5-Catalysts deactivation and regeneration, in: S. Joshi, V. Ranade (Eds.) Industrial Catalytic Processes for Fine and Specialty Chemicals, Elsevier, 2016, pp.187–219. https://doi.org/10.1016/B978-0-12-801457-8.00005-7

[18] H.S. Bengaard, J.K. Norskov, J. Sehested, B.S. Clausen, L.P. Nielsen, A.M. Molenbroek, J.R. Rostrup-Nielsen, Steam reforming and graphite formation on Ni catalysts, J. Catal. 209 (2002) 365–384. https://doi.org/10.1006/jcat.2002.3579

[19] Z. Alipour, M. Rezaei, F. Meshkani, Effect of alkaline earth promoters (MgO, CaO, and BaO) on the activity and coke formation of Ni catalysts supported on nanocrystalline Al_2O_3 in dry reforming of methane, J. Ind. Eng. Chem. 20 (2014) 2858–2863. https://doi.org/10.1016/j.jiec.2013.11.018

[20] C.J. Liu, J. Ye, J. Jiang, Y. Pan, Progresses in the preparation of coke resistant Ni-based catalyst for steam and CO_2 reforming of methane, ChemCatChem 3 (2011) 529–541. https://doi.org/10.1002/cctc.201000358

[21] B. Valle, A. Remiro, A.T. Aguayo, J. Bilbao, A.G. Gayubo, Catalysts of $Ni/\alpha\text{-}Al_2O_3$ and $Ni/La_2O_3\text{-}\alpha Al_2O_3$ for hydrogen production by steam reforming of bio-oil aqueous fraction with pyrolytic lignin retention, Int. J. Hydrogen Energy 38 (2013) 1307–1318. https://doi.org/10.1016/j.ijhydene.2012.11.014

[22] A. Ochoa, B. Aramburu, B. Valle, D.E. Resasco, J. Bilbao, A.G. Gayubo, P. Castaño, Role of oxygenates and effect of operating conditions in the deactivation of a Ni supported catalyst during the steam reforming of bio-oil, Green Chem. 19 (2017) 4315–4333. https://doi.org/10.1039/C7GC01432E

[23] B. Valle, B. Aramburu, M. Olazar, J. Bilbao, A.G. Gayubo, Steam reforming of raw bio-oil over $Ni/La_2O_3\text{-}\alpha Al_2O_3$: Influence of temperature on product yields and catalyst deactivation, Fuel 216 (2018) 463–474. https://doi.org/10.1016/j.fuel.2017.11.149

[24] A. Remiro, B. Valle, A.T. Aguayo, J. Bilbao, A.G. Gayubo, Operating conditions for attenuating Ni/La_2O_3-αAl_2O_3 catalyst deactivation in the steam reforming of bio-oil aqueous fraction, Fuel Process. Technol. 115 (2013) 222–232. https://doi.org/10.1016/j.fuproc.2013.06.003

[25] B. Valle, B. Aramburu, P.L. Benito, J. Bilbao, A.G. Gayubo, Biomass to hydrogen-rich gas via steam reforming of raw bio-oil over Ni/La_2O_3-αAl_2O_3 catalyst: Effect of space-time and steam-to-carbon ratio, Fuel 216 (2018) 445–455. https://doi.org/10.1016/j.fuel.2017.11.151

[26] J. Sehested, J.A.P. Gelten, I.N. Remediakis, H. Bengaard, J.K. Norskov, Sintering of nickel steam-reforming catalysts: effects of temperature and steam and hydrogen pressures, J. Catal. 223 (2004) 432–443. https://doi.org/10.1016/j.jcat.2004.01.026

[27] J. Sehested, J.A.P. Gelten, S. Helveg, Sintering of nickel catalysts: Effects of time, atmosphere, temperature, nickel-carrier interactions, and dopants, Appl. Catal. A-Gen. 309 (2006) 237–246. https://doi.org/10.1016/j.apcata.2006.05.017

[28] A. Remiro, B. Valle, A.T. Aguayo, J. Bilbao, A.G. Gayubo, Steam reforming of raw bio-oil in a fluidized bed reactor with prior separation of pyrolytic lignin, Energy Fuels 27 (2013) 7549–7559. https://doi.org/10.1021/ef401835s

[29] T. Davidian, N. Guilhaume, E. Iojoiu, H. Provendier, C. Mirodatos, Hydrogen production from crude pyrolysis oil by a sequential catalytic process, Appl. Catal. B-Environ. 73 (2007) 116–127. https://doi.org/10.1016/j.apcatb.2006.06.014

[30] C. Wu, R. Liu, R. Sustainable hydrogen production from steam reforming of bio-oil model compound based on carbon deposition/elimination, Int. J. Hydrogen Energy 36 (2011) 2860–2868. https://doi.org/10.1016/j.ijhydene.2010.11.113

[31] F. Lónyi, J. Valyon, E. Someus, J. Hancsók, Steam reforming of bio-oil from pyrolysis of MBM over particulate and monolith supported Ni/α-Al_2O_3 catalysts, Fuel 112 (2013) 23–30. https://doi.org/10.1016/j.fuel.2013.05.010

[32] A. Remiro, A. Arandia, L. Oar-Arteta, J. Bilbao, A.G. Gayubo, Regeneration of $NiAl_2O_4$ spinel type catalysts used in the reforming of raw bio-oil, Appl. Catal. B-Environ. 237 (2018) 353–365. https://doi.org/10.1016/j.apcatb.2018.06.005

[33] A. Remiro, A. Arandia, J. Bilbao, A.G. Gayubo, Comparison of Ni based and Rh based catalyst performance in the oxidative steam reforming of raw bio-oil, Energy Fuels 31 (2017) 7147–7156. https://doi.org/10.1021/acs.energyfuels.7b00735

[34] A. Arandia, A. Remiro, V. García, P. Castaño, J. Bilbao, A.G. Gayubo, Oxidative steam reforming of raw bio-oil over supported and bulk Ni catalysts for hydrogen production, Catalysts 8 (2018) nº 322. https://doi.org/10.3390/catal8080322

[35] A. Al-Ubiad, E.E. Wolf, Steam reforming of methane on reduced non-stoichiometric nickel aluminate catalysts, Appl. Catal. 40 (1988) 73–85. https://doi.org/10.1016/S0166-9834(00)80427-3

[36] L. García, M.L. Salvador, J. Arauzo, R. Bilbao, CO_2 as a gasifying agent for gas production from pine sawdust at low temperatures using a Ni/Al coprecipitated catalyst, Fuel Process. Technol. 69 (2001) 157–174. https://doi.org/10.1016/S0378-3820(00)00138-7

[37] B. Valle, B. Aramburu, A. Arandia, A. Remiro, J. Bilbao, A.G. Gayubo. Optimal Conditions of Thermal Treatment Unit for the Steam Reforming of Raw Bio-oil in a Continuous Two-step Reaction System, Chem. Eng. Trans. 57 (2017) 205–210. https://doi.org/10.3303/CET1757035

[38] A. Arandia, A. Remiro, L. Oar-Arteta, J. Bilbao, A.G. Gayubo. Reaction conditions effect and pathways in the oxidative steam reforming of raw bio-oil on a Rh/CeO_2-ZrO_2 catalyst in a fluidized bed reactor, Int. J. Hydrogen Energy 42 (2017) 29175–29185. https://doi.org/10.1016/j.ijhydene.2017.10.095

[39] R. Kumar, N. Enjamuri, S. Shah, A.S. Al-Fastesh, J.J. Bravo-Suárez, B. Chowdhury, Ketonization of oxygenated hydrocarbons on metal oxide based catalysts, Catal. Today 302 (2018) 16–49. https://doi.org/10.1016/j.cattod.2017.09.044

[40] B. Valle, B. Aramburu, C. Santiviago, J. Bilbao, A.G. Gayubo, Upgrading of bio-oil in continuous process with dolomite catalysts, Energy Fuels 28 (2014) 6419–6428. https://doi.org/10.1021/ef501600f

[41] F. Bimbela, D. Chen, J. Ruiz, L. García, J. Arauzo, Ni/Al coprecipitated catalysts modified with magnesium and copper for the catalytic steam reforming of model compounds from biomass pyrolysis liquids, Appl. Catal. B-Environ. 119–120 (2012) 1–12. https://doi.org/10.1016/j.apcatb.2012.02.007

[42] A. Ochoa, B. Valle, D.E. Resasco, J. Bilbao, A.G. Gayubo, P. Castaño, Temperature programmed oxidation coupled with in situ techniques reveal the nature and location of coke deposited on a Ni/La_2O_3-αAl_2O_3 catalyst in the steam reforming of bio-oil, ChemCatChem 10 (2018) 2311–2321. https://doi.org/10.1002/cctc.201701942

[43] Z. Zhang, X. Hu, J. Li, G. Gao, D. Dong, R. Westerhof, S. Hu, J. Xiang, Y. Wang, Steam reforming of acetic acid over Ni/Al2O3 catalysts: Correlation of nickel loading with properties and catalytic behaviors of the catalysts, Fuel 217 (2018) 389–403. https://doi.org/10.1016/j.fuel.2017.12.114

[44] J.A. Medrano, M. Oliva, J. Ruiz, L. García, J. Arauzo, Hydrogen from aqueous fraction of biomass pyrolysis liquids by catalytic steam reforming in fluidized bed, Energy 36 (2011) 2251–2224. https://doi.org/10.1016/j.energy.2010.03.059

[45] C. Italiano, K. Bizkarra, V.L. Barrio, J.F. Cambra, L. Pino, A. Vita, Renewable hudrogen production via steam reforming of simulated bio-oil over Ni-based catalysts, Int. J. Hydrogen Energy 44 (2019) 14671–14682. https://doi.org/10.1016/j.ijhydene.2019.04.090

[46] J.W. Snoeck, G.F. Froment, M. Fowles, Steam/CO_2 reforming of methane. Carbon filament formation by the boudouard reaction and gasification by CO_2, by H_2, and by steam: Kinetic study, Ind. Eng. Chem. Res. 41 (2002) 4252–4265. https://doi.org/10.1021/ie010666h

[47] J. Vicente, C. Montero, J. Ereña, M.J. Azkoiti, J. Bilbao, A.G. Gayubo, Coke deactivation of Ni and Co catalysts in ethanol steam reforming at mild temperatures in a fluidized bed reactor, Int. J. Hydrogen Energy 39 (2014) 12586−12596. https://doi.org/10.1016/j.ijhydene.2014.06.093

[48] C. Montero, A. Ochoa, P. Castaño, J. Bilbao, A.G. Gayubo, Monitoring Ni^0 and coke evolution during the deactivation of a Ni/La_2O_3-αAl_2O_3 catalyst in ethanol steam reforming in a fluidized bed, J. Catal. 331 (2015) 181–192. https://doi.org/10.1016/j.jcat.2015.08.005

[49] L.S. Lobo, J.L. Figueiredo, C.A. Bernardo, Carbon formation and gasification on metals. Bulk diffusion mechanism: A reassessment, Catal. Today 178 (2011) 110–116. https://doi.org/10.1016/j.cattod.2011.07.030

[50] J.L. Pinilla, I. Suelves, M.J. Lázaro, R. Moliner, J.M. Palacios, Activity of NiCuAl catalyst in methane decomposition studied using a thermobalance and the structural changes in the Ni and the deposited carbon, Int. J. Hydrogen Energy 33 (2008) 2515–2524. https://doi.org/10.1016/j.ijhydene.2008.02.041

[51] M. Nasir Uddin, W.M.A. Wan Daud, H.F. Abbas, Kinetics and deactivation mechanisms of the thermal decomposition of methane in hydrogen and carbon nanofiber Co-production over Ni-supported Y zeolite-based catalysts, Energ. Convers. Manage. 87 (2014) 796–809. https://doi.org/10.1016/j.enconman.2014.07.072

[52] S. Wang, G.Q. Lu, A comprehensive study on carbon dioxide reforming of methane over Ni/γ-Al_2O_3 catalysts, Ind. Eng. Chem. Res. 38 (1999) 2615–2625. https://doi.org/10.1021/ie980489t

[53] M. Bilal, S.D. Jackson, Steam reforming of ethanol at medium pressure over Ru/Al_2O_3: effect of temperature and catalyst deactivation, Catal. Sci. Technol. 2 (2012) 2043–2051. https://doi.org/10.1039/C2CY20267K

[54] K.M. Hardiman, C.G. Cooper, A.A. Adesina, R. Lange, Post-mortem characterization of coke-induced deactivated alumina-supported Co–Ni catalysts, Chem. Eng. Sci. 61 (2006) 2565–2573. https://doi.org/10.1016/j.ces.2005.11.021

[55] M.D. Argyle, C. Bartholomew, Heterogeneous catalyst deactivation and regeneration: A review, Catalysts 5 (2015) 145–269. https://doi.org/10.3390/catal5010145

[56] A.G. Gayubo, J. Vicente, J. Ereña, C. Montero, M. Olazar, J. Bilbao, Comparison of Ni and Co catalysts for ethanol steam reforming in a fluidized bed reactor, Catal. Lett. 144 (2014) 1134–1143. https://doi.org/10.1007/s10562-014-1265-x

[57] D. Gómez-Gualdrón, P. Balbuena, Characterization of carbon atomistic pathways during single-walled carbon nanotube growth on supported metal nanoparticles, Carbon 57 (2013) 298–309. https://doi.org/10.1016/j.carbon.2013.01.077

[58] F.R. Shamskar, M. Rezaei, F. Meshkani, The influence of Ni loading on the activity and coke formation of ultrasound-assisted co-precipitated Ni-Al_2O_3 nanocatalyst in dry reforming of methane, Int. J. Hydrogen Energy 42 (2017) 4155–4164. https://doi.org/10.1016/j.ijhydene.2016.11.067

Figure Captions

Figure 1. Evolution with TOS of bio-oil oxygenates conversion and products yields. Reaction conditions: 700 ºC; S/C, 6; O/C, 0.34; space time, 0.15 $g_{catalyst}h \cdot g_{bio\text{-}oil}^{-1}$.

Figure 2. TPO profiles (a), total coke content and cokes I-II fractions (b) for the catalyst used at different TOS. Reaction conditions: 700 ºC; S/C, 6; O/C, 0.34; space time, 0.15 $g_{catalyst}h \cdot g_{bio\text{-}oil}^{-1}$.

Figure 3. TEM images of fresh-reduced and samples of catalyst used at different TOS. Reaction conditions: 700 ºC; S/C, 6; O/C, 0.34; space time, 0.15 $g_{catalyst}h \cdot g_{bio\text{-}oil}^{-1}$.

Figure 4. Particle size distribution (PSD) of Ni^0 crystals and average particle size obtained from TEM images of fresh-reduced and samples of catalyst used at different TOS Reaction conditions: 700 ºC; S/C, 6; O/C, 0.34; space time, 0.15 $g_{catalyst}h \cdot g_{bio\text{-}oil}^{-1}$.

Figure 5. Deactivation scheme of catalyst based on Ni morphological changes and coke evolution with TOS. Reaction conditions: 700 ºC; S/C, 6; O/C, 0.34; space time, 0.15 $g_{catalyst}h \cdot g_{bio\text{-}oil}^{-1}$.

Tables

Table 1. Yield and composition of oxygenates (on a water-free basis) in the raw bio-oil, in the stream that enters the OSR reactor**,** and in the liquid produced at different TOS values. Reaction conditions: 700 ºC; S/C, 6; O/C, 0.34; space time, 0.15 $g_{catalyst}h \cdot g_{bio\text{-}oil}^{-1}$.

Table 2. Physical properties of fresh-reduced and samples of catalyst used at different TOS. Reaction conditions: 700 ºC; S/C, 6; O/C, 0.34; space time, 0.15 $g_{catalyst}h \cdot g_{bio\text{-}oil}^{-1}$.

Table 3. Evolution with TOS of the average Ni particle size, estimated by XRD diffractograms in the diffraction angle 51.8 º (plane 2 0 0). Reaction conditions: 700 ºC; S/C, 6; O/C, 0.34; space time, 0.15 $g_{catalyst}h \cdot g_{bio\text{-}oil}^{-1}$.